**Matter, Volume *4***

## Supplemental information

# Integrated contact lens sensor system based on multifunctional ultrathin $MoS_2$ transistors

**Shiqi Guo, Kaijin Wu, Chengpan Li, Hao Wang, Zheng Sun, Dawei Xi, Sheng Zhang, Weiping Ding, Mona E. Zaghloul, Changning Wang, Fernando A. Castro, Dong Yang, and Yunlong Zhao**

## Supplemental Information

**Table S1. Comparison of the PDMS with other commercial materials used for contact lenses substrate.**

| Contact Lens Substrate | Pros | Cons |
|---|---|---|
| PDMS | Elastic, gas-permeable, biocompatible, low-cost, easy manufacturing | Low hydrophilicity, protein accumulation |
| PVA | Low-cost, biocompatible, easy manufacturing | Low gas-permeable, fixed water recipe |
| Hydrogel | Elastic, copolymer possibilities | Easily abrasive, comonomer |
| HEMA | Low-cost, biocompatible | Low gas-permeable, protein accumulation |
| PMMA | Low-cost, well-understood polymer | No gas-permeable, rigid |
| RGP | Gas-permeable, long-lasting | Expensive, easily abrasive |
| Silicone | Gas-permeable, long-lasting | Expensive, easily abrasive |

**Table S2. Performance comparison of several representative glucose sensors**

| Sensor | Type | Linear Range (mM) | Sensitivity ($\mu A/cm^2 mM$) | Reference |
|---|---|---|---|---|
| GOx/$MoS_2$ | Enzyme | 0->1 | 1794.4 | This work |
| $Cu_2O/MoS_2$ | Non-enzyme | 0.01-4 | 3108.87 | Fang et al. 2017 [S1] |
| GOx/ZnO/Au | Enzyme | 0.01-3.45 | 23.1 | Wei et al. 2006 [S2] |
| GOx/ZnO | Enzyme | Not mentioned | 21 | Ren et al. 2009 [S3] |
| GOx/BSA/Nafion/ZnO nanorode/GE | Enzyme | 0.6–1.4 | 10.911 | Marie et al. 2015 [S4] |
| GOx/Cu/MWCNTs | Enzyme | 0.7–3.5 | 251.4 | Kang et al. 2007 [S5] |
| ZnO nanoparticle | Non-enzyme | 1–10 | 38.133 | Singh et al. 2012 [S6] |
| GC/Cu-$Ag_2O$ NW | Non-enzyme | 200-3200 | 298.2 | Fang et al. 2009 [S7] |

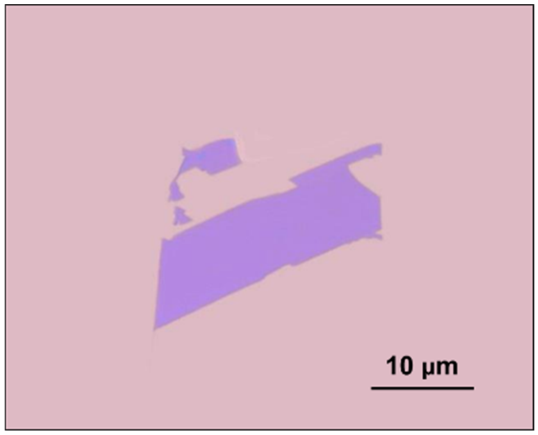


7

8 **Figure S1. Representative optical image of $MoS_2$ flake obtained via traditional mechanical**
9 **exfoliation method.**

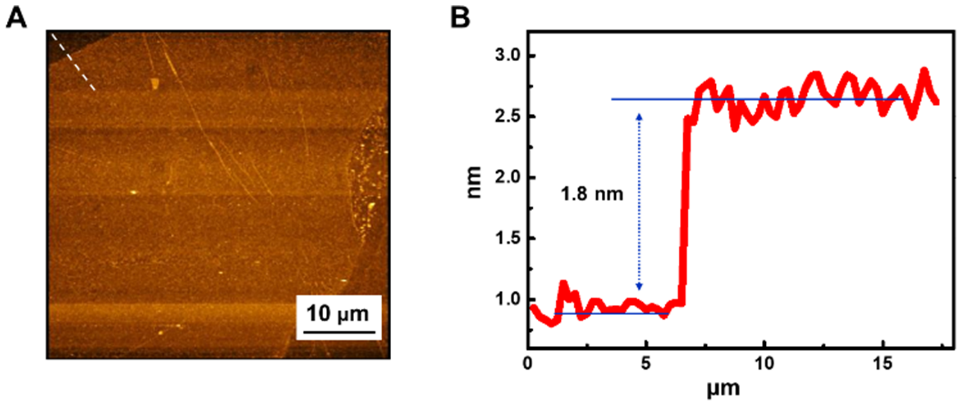


**Figure S2. Thickness characteristics of the $MoS_2$ flake.** (A) AFM image and (B) height profile showing the thickness of 1.8 nm.

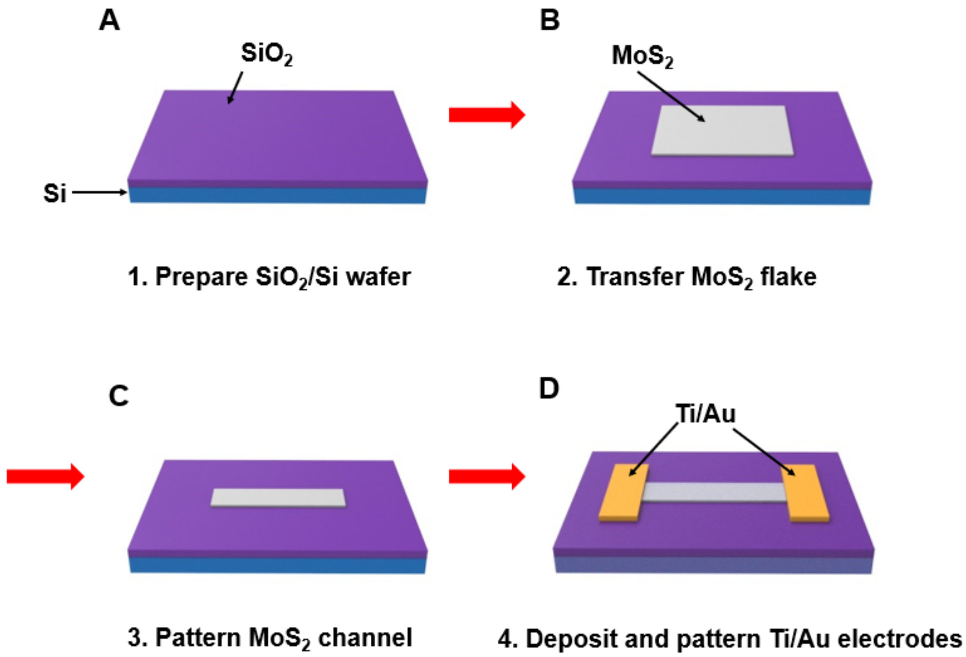


**Figure S3. The fabrication process of the FET on the $SiO_2$/Si substrate.** (A) Clean the $SiO_2$/Si wafer with the standard cleaning process. (B) Exfoliate $MoS_2$ flake onto the surface of the substrate. (C) Pattern $MoS_2$ as the active channel with $O_2$ and $SF_6$ plasma. (D) E-beam deposit and pattern Ti/Au (5 nm/150 nm) source and drain electrodes.

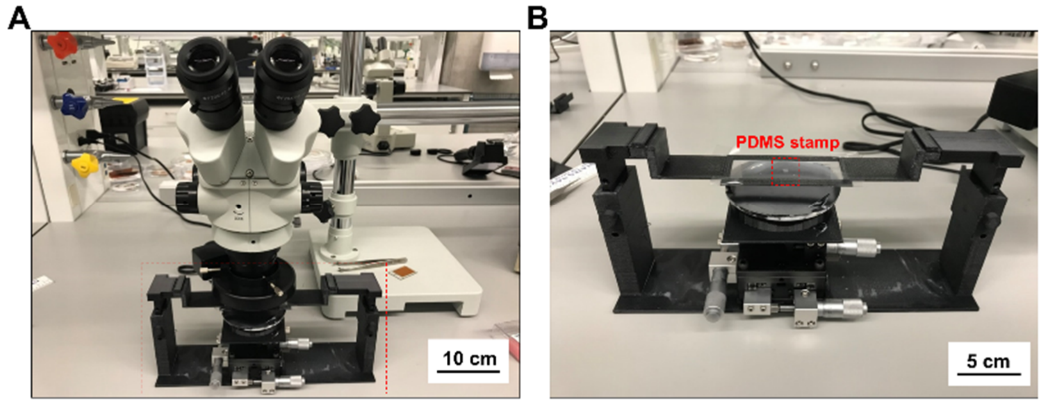


**Figure S4. The experimental setup for the transfer printing process of $MoS_2$ transistor.** (A) Optical microscope for alignment. (B) PDMS stamp on glass slides for $MoS_2$ transfer.

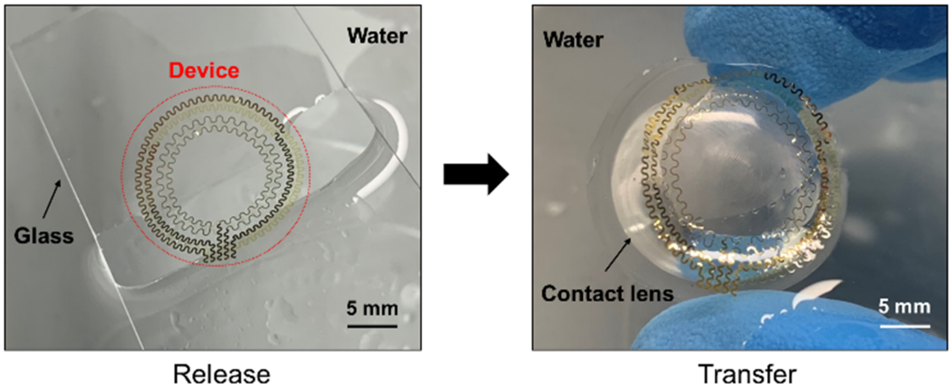


**Figure S5. Photographs for releasing the sensor layer from the glass substrate and transferring it onto the PDMS contact lens substrate.**

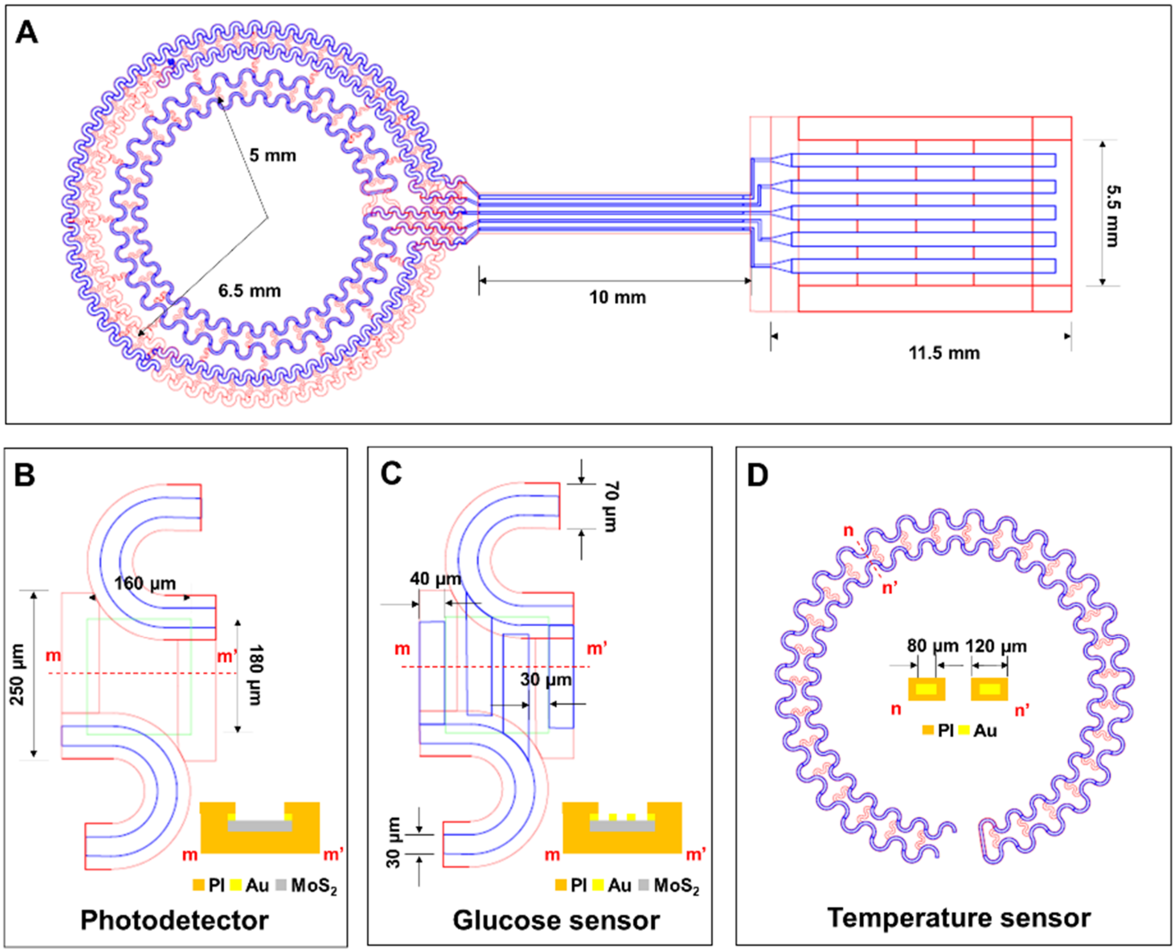


**Figure S6. Design of the entire system including the external connection, the blue line as the metal electrode and red line as PI.** (A) The overview architecture of the system. (B) The schematic details of the photodetector and the inset showing the cross-sectional view of the structure. (C) The geometrical details of the glucose sensor. (D) The flat structure details of the temperature sensor.

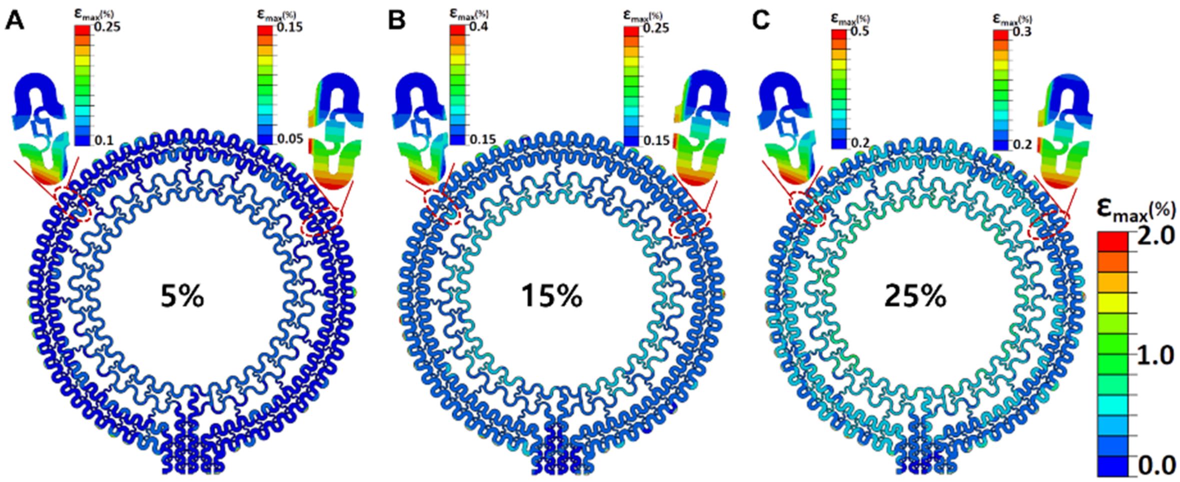


**Figure S7. The finite element analysis (FEA) of the sensor system with the device under biaxial radial strain.** (A) Under a strain of 5%. (B) Under a strain of 15%. (C) Under a radial of 25%. The maximum principal strains are below 2.0 %.

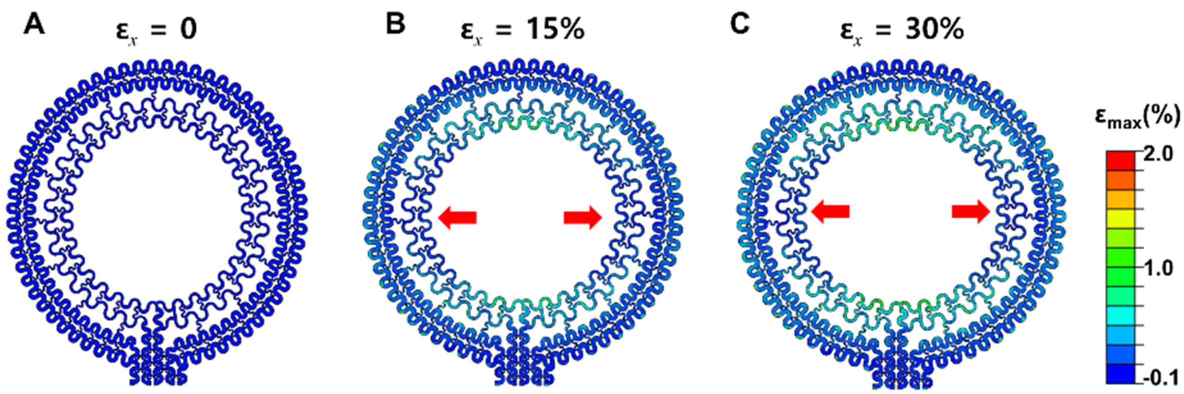


**Figure S8. The FEA of the sensor system with the device under a uniaxial (X-axis) tensile.** (A) The original state. (B) Under a strain of 15%. (C) Under a strain of 30%. The maximum principal strains are below 2.0 %.

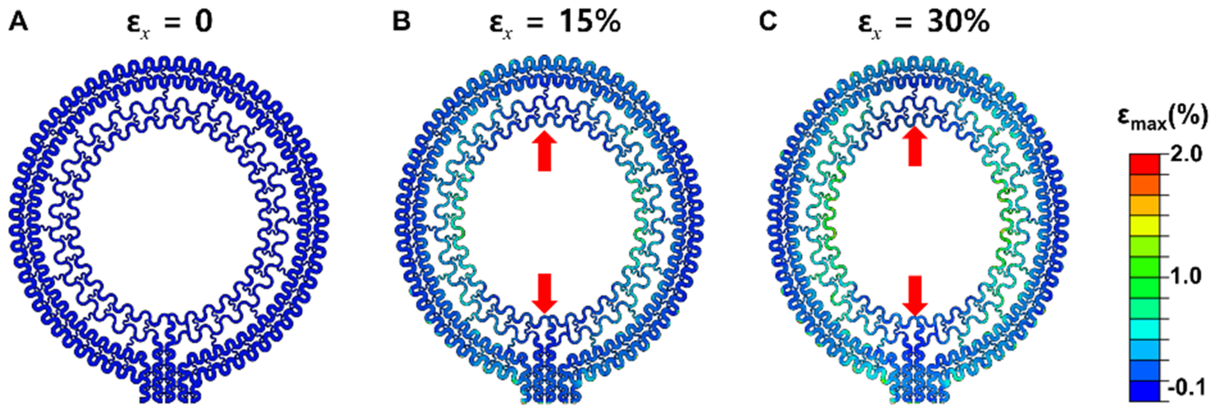


**Figure S9. The FEA of the sensor system with the device under a Y-axis tensile.** (A) The original state. (B) Under a strain of 15%. (C) Under a strain of 30%. The maximum principal strains are below 2.0 %.

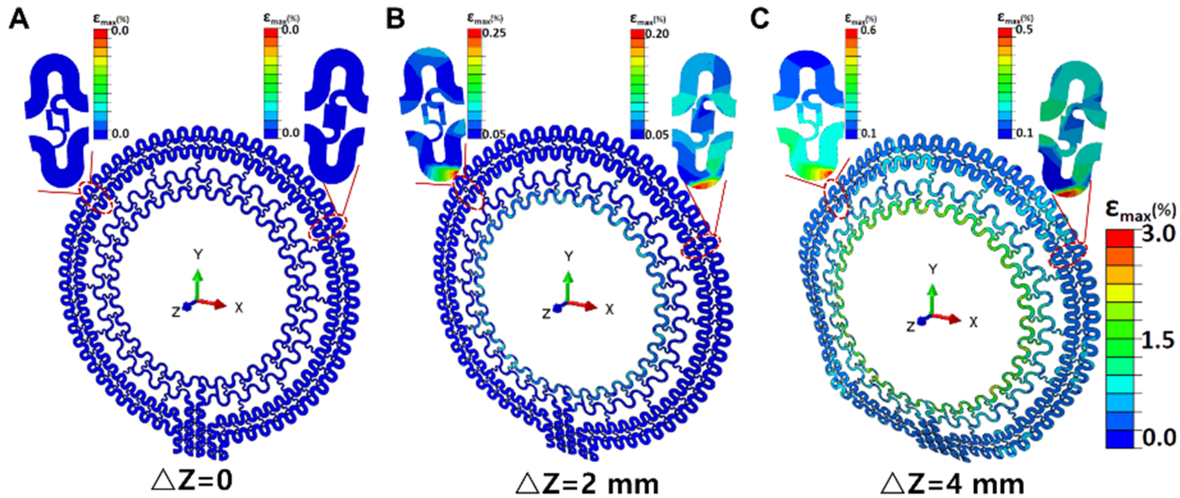


**Figure S10. The FEA of the sensor system with the increasing of Z-displacement.** (A) with Z-displacement of 0 mm, (B) with Z-displacement of 2 mm to (C) with Z-displacement of 4 mm. The maximum principal strains remain < 3.0 %.

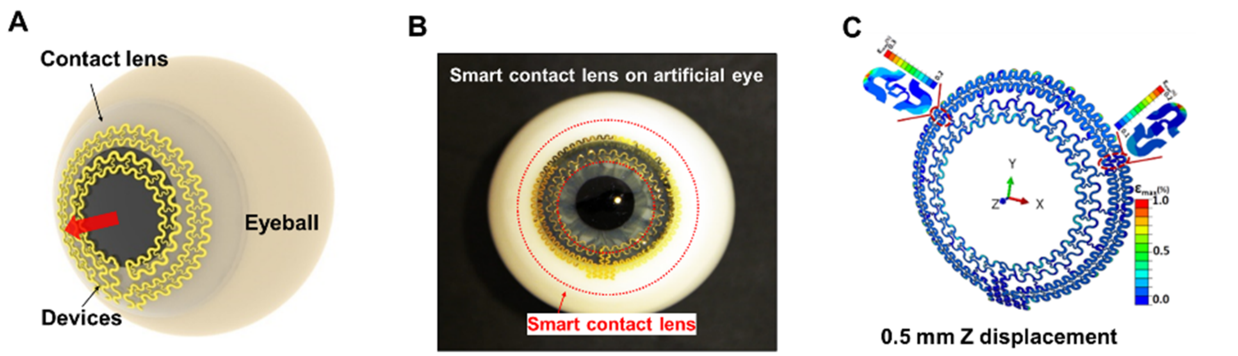


**Figure S11. Illustration, optical image and FEA performed on the system with the lens on an artificial eyeball.** (A) Schematic illustration and (B) optical image the contact lens wearing on an artificial eyeball. (C) FEA strain map with Z-displacement of 0.5 mm. The maximum principal strains remain < 1.0%.

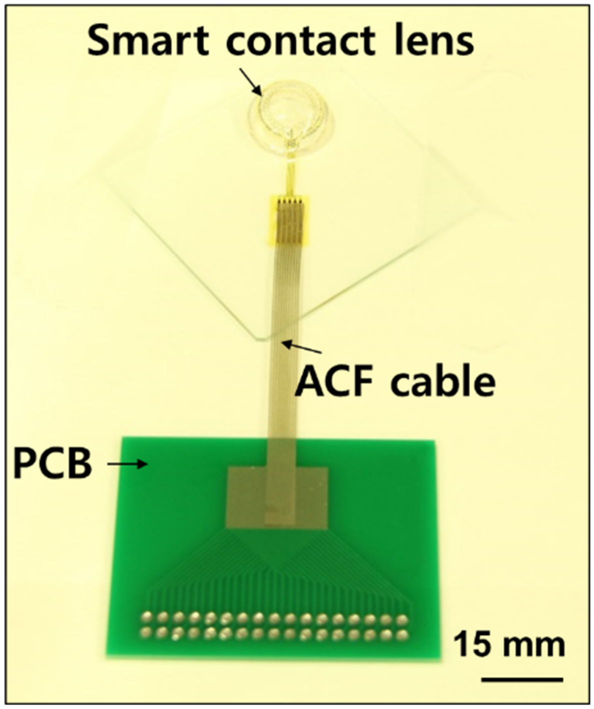


**Figure S12. Photograph of smart contact lens after connecting with an external print circuit board (PCB) through an anisotropic conductive film (ACF) cable.**

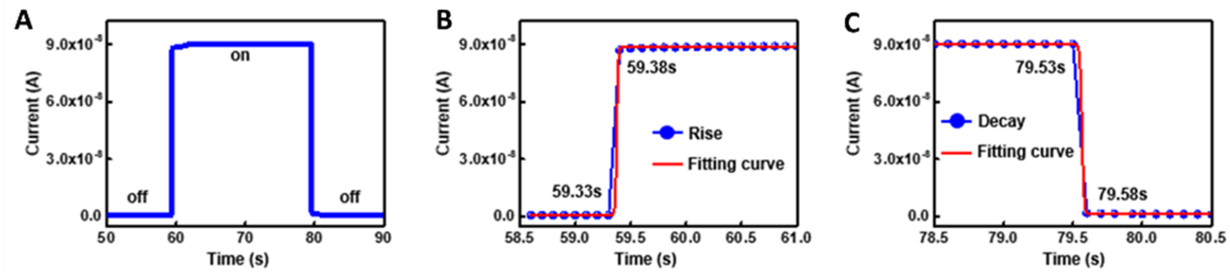


**Figure S13. The magnified plot of one response cycle and the rise and decay curve.** (A) Magnified plot of one response cycle by illumination via UV light at a bias of 3 V. (B) Sigmoid curve fitting of the rise showing ~ 50 ms rise time. (C) Sigmoid curve fitting of the decay showing ~ 50 ms decay time.

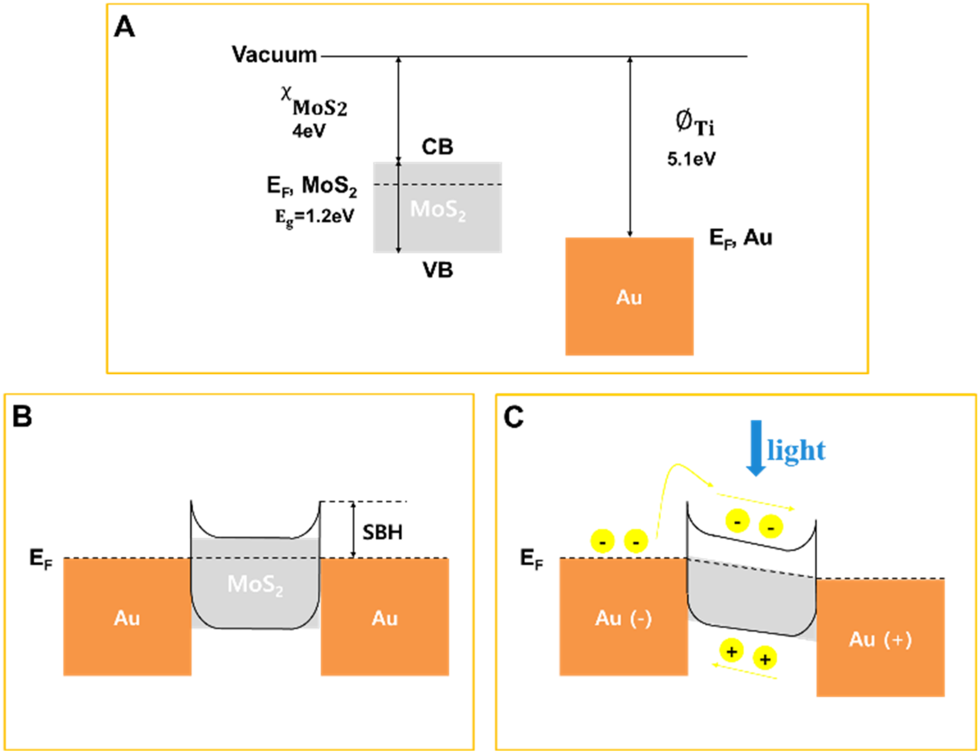


**Figure S14. Energy band diagrams showing the mechanism of $MoS_2$ photodetector.** (A) The band diagrams of separate $MoS_2$ and gold, corresponding to the vacuum level. (B) Illustration for the band alignment between electrodes and $MoS_2$ channel with the Schottky barrier height (SBH). (C) After bias and light are applied, the electrons are excited and moved to the conduction band, resulting in higher current flow.

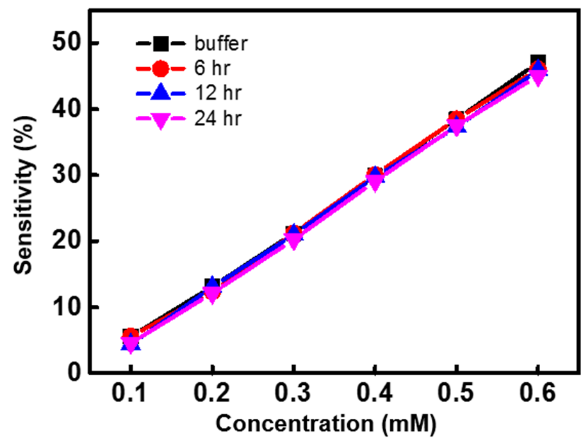


**Figure S15. Stability test of the glucose sensor with various concentrations of glucose in artificial tear and for different storage times, up to 24 hours.**

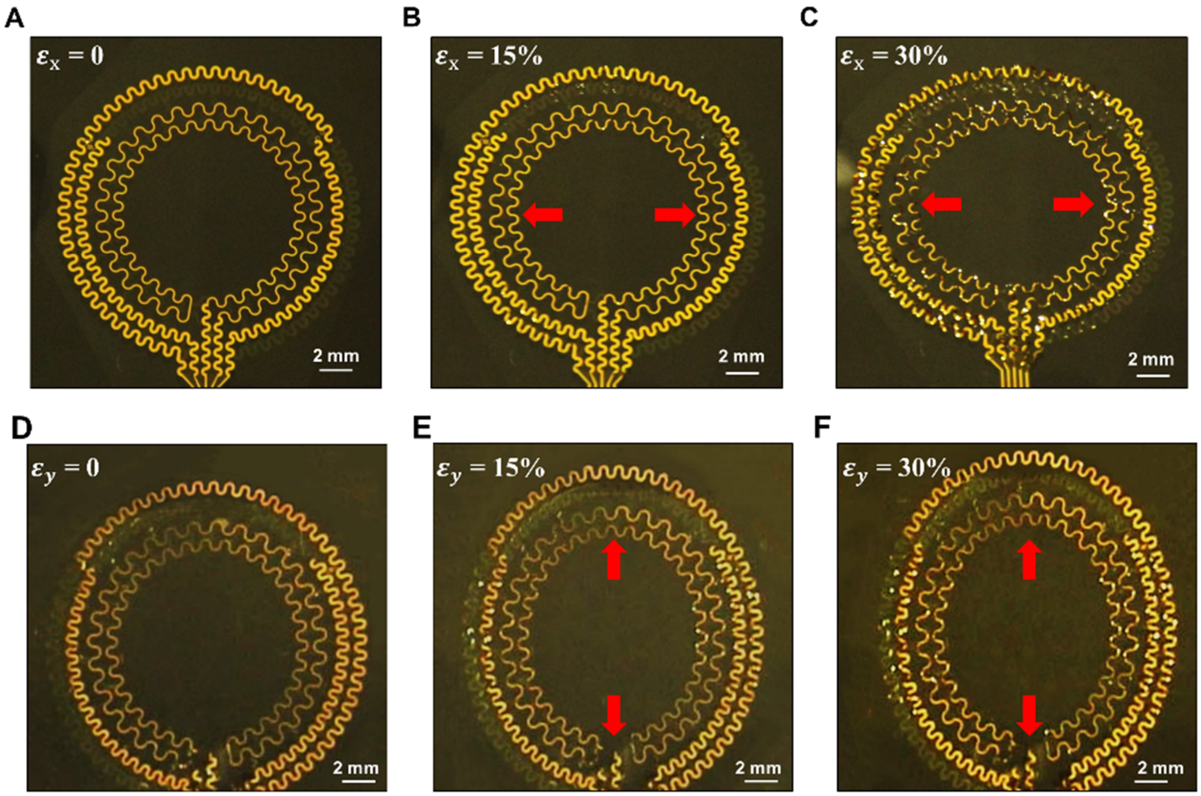


**Figure S16. Photographs of the smart contact lens stretched under uniaxial tensile stress.** (A-C) Photographs of the stretched device at the original state and under uniaxial (X-axis) tensile strain of 15% and 30%. (D-F) The photograph of the stretched device at the original state and under uniaxial (Y-axis) tensile strain of 15% and 30%. Due to the curvature of the lens, parts of the sensor may come out of the camera focus during stretch, which leads to parts of the electrodes to be less visible in some images.

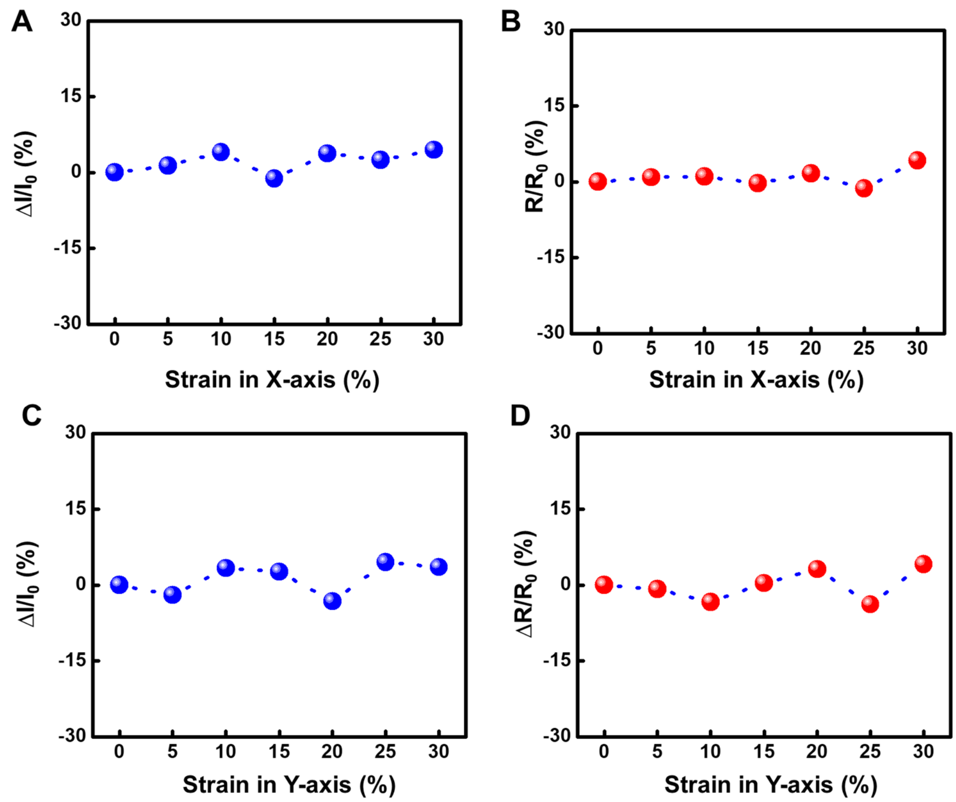


**Figure S17. The sensing properties of the stretched device under uniaxial tensile**. (A, B) Relative changes in current as a function of the X-axis tensile strain up to 30% for the UV response (A) and glucose response (B). (C, D) Relative changes in current as a function of the Y-axis tensile strain up to 30% for the UV response (C) and glucose response (D).

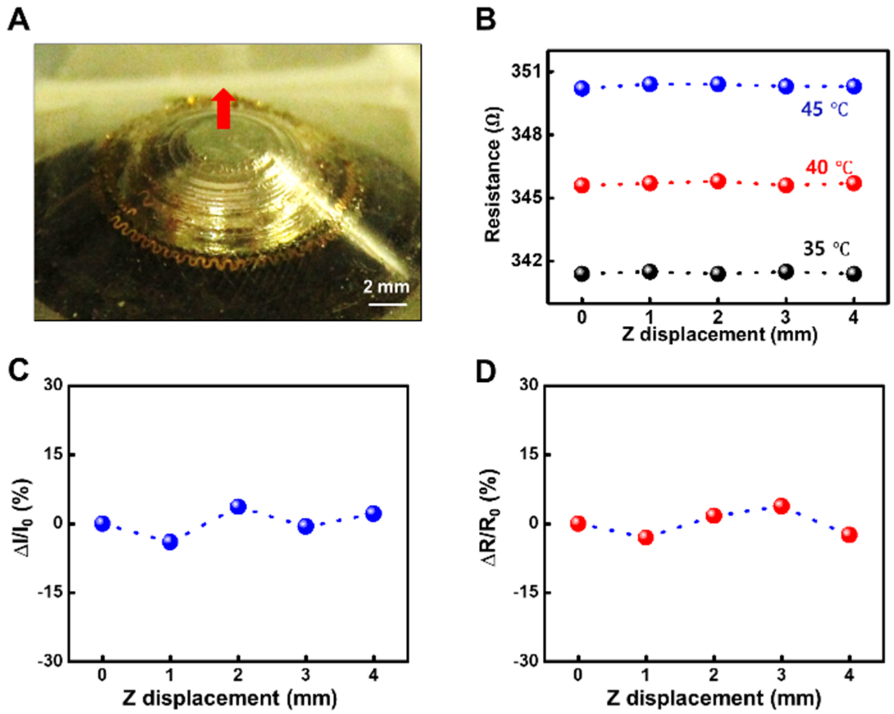


**Figure S18. The photograph and sensing properties of the stretched device under Z displacement.** (A) The photograph of the device under a Z-axis displacement of 4 mm from the centre. (B) The resistance of the temperature sensor versus Z-axis displacement under different temperatures. (C, D) Relative changes in current as a function of Z-axis displacement for the UV response (C) and glucose response (D).

## References:

S1. Fang, L., Wang, F., Chen, Z., Qiu, Y., Zhai, T., Hu, M., Zhang, C., and Huang, K. (2017). Flower-like $MoS_2$ decorated with $Cu_2O$ nanoparticles for non-enzymatic amperometric sensing of glucose. Talanta *167*, 593-599.

S2. A. Wei, X.W.S., J. X. Wang, Y. Lei, X. P. Cai, C. M. Li, Z. L. Dong, and W. Huang (2006). Enzymatic glucose biosensor based on ZnO nanorod array grown by hydrothermal decomposition. Applied Physics Letter *89*, 123902.

S3. Ren, X., Chen, D., Meng, X., Tang, F., Hou, X., Han, D., and Zhang, L. (2009). Zinc oxide nanoparticles/glucose oxidase photoelectrochemical system for the fabrication of biosensor. J Colloid Interface Sci *334* (2), 183-187.

S4. Marie, M., Mandal, S., and Manasreh, O. (2015). An Electrochemical Glucose Sensor Based on Zinc Oxide Nanorods. Sensors (Basel) *15* (8), 18714-18723.

S5. Kang, X., Mai, Z., Zou, X., Cai, P., and Mo, J. (2007). A sensitive nonenzymatic glucose sensor in alkaline media with a copper nanocluster/multiwall carbon nanotube-modified glassy carbon electrode. Anal Biochem *363* (1), 143-150.

S6. Singh, K.; Umar, A.; Kumar, A.; Chaudhary, G.R.; Singh, S.; Mehta, S.K. (2012) Non-enzymatic glucose sensor based on well-crystallized ZnO nanoparticles. Sci. Adv. Mater. 2012, *4* (9), 994–1000.

S7. Fang, B., Gu, A., Wang, G., Wang, W., Feng, Y., Zhang, C., and Zhang, X. (2009). Silver oxide nanowalls grown on Cu substrate as an enzymeless glucose sensor. ACS Appl Mater Interfaces *1* (12), 2829-2834.